THE EFFECT OF INITIAL CONDITIONS ON ISOTROPIC TURBULENCE

P. Orlandi
Dipartimento di Meccanica e Aeronautica
Università La Sapienza
Via Eudosiana 16, I-00184, Roma
email orlandi@dma.ing.uniroma1.it

F. Fabiani
Avio S.p.A.
email fabrizio.fabiani@aviogroup.com

ABSTRACT

The difficulties in laboratory experiments in understanding the vortex dynamics in the region between the grid and that where isotropic turbulence is obtained suggest to perform direct numerical simulations. In this paper flows with analytical inlet disturbances are compared with those obtained by simulating flows past real grids. The results show that the turbulent energy decay rate ($q \approx x_1^{-m}$) depends on the shape of the grid. The analysis is focused on analytical disturbances and in particular by considering $-\langle Q \rangle = \langle s_{ij}s_{ji} \rangle - \langle \omega_i\omega_i/2 \rangle$ and the terms in the U_1 momentum equation written in rotational form. The energy spectra compare well with those in forced simulations, in addition it has been observed that, at the same *Re* number the multiple scale disturbances generate flows at R_λ higher than those with single scale disturbances.

INTRODUCTION

The complex flow physics of turbulent flows has been studied in isotropic turbulence. In this flow the turbulent kinetic energy $q = \langle u_i^2 \rangle/2$ decays in time as t^{-m}. The $\langle\rangle$ indicates averages in the homogeneous directions. This flow, in a laboratory, is generated by inserting in wind tunnels grids whose solidity produce a flow with energy spectra peaked at a wave number related to the mesh size M of the grid. The flow is not isotropic in the region behind the grid, for the effect of the flow structures generated on the solid surface of the grid, and becomes isotropic downstream, within a distance function of M. The flow reaches a statistical stationary steady state, with q varying in the downstream direction x_1 in a complex way. Batchelor & Townsend (1948a, 1948b) in two papers observed that the energy was decaying with a power law x_1^{-m}, with $m = 1$ in the initial and $m = 5/2$ in the final period. The dependence of m on the shape of the grid has not fully understood, however it can be presumed that the value of m in the initial period is related to the vortical structures generated by the grid, and it is important to establish how far downstream the initial conditions affect the turbulence. In a laboratory the full comprehension of the link between m and the initial conditions can not be achieved for the difficulty to measure the vorticity field. Recent experiments by Lavoie *et al.*(2007) and Seoud & Vassilicos (2007) were devoted to investigate the influence of the shape of the grid on the power law decay. In a more recent paper, Ertunc *et al.*(2010) reporting laboratory and numerical experiments, listed the experimental requirements to generate homogeneous flows.

The numerical simulation may help to understand the flow physics, for the possibility to have any quantity and in particular pressure and vorticity fields. In the past simulations of isotropic decaying turbulence at $t = 0$ assigned velocity components with random phases and energy spectra peaked at different wave number. These initial conditions, having random phases, differ from those in the real experiments and then the effects of the vortical structures can not be studied. To help the experimentalist the simulations should mimic, as much as possible, the conditions obtained in wind tunnels by inserting grids after the contraction. Regular square grids are often used, therefore Djenidi (2006) and Ertunc *et al.*(2010) could use the lattice Boltzman method to reproduce the flow past biplane grids. Djenidi (2006) was not interested to analyse the effects of the grid solidity, which on the other hand was investigated Ertunc *et al.*(2010).

By using multiscale grids Seoud & Vassilicos (2007) and Hurst & Vassilicos (2007) produced flows with unusual turbulence properties. Also for multiple scale configurations the rate of energy dissipation ($\varepsilon = 2\nu S$, with $S = \langle s_{ij}s_{ji} \rangle$) dictates the energy decay rate. Since ε is linked to the vortical structures generated by the grid its shape controls the distance where the flow becomes isotropic. A careful analysis of the flow structures in the anisotropic region by DNS with different inlet conditions allows to understand how to obtain the desired isotropic turbulence.

As before mentioned for the single-scale disturbances the comprehension of the interaction among flow-structures of different size in the region past and close to the grid is rather difficult in experimental studies. In presence of multiscale-scale grids the analysis is even more difficult and the DNS could be of help. The numerical reproduction of the fractal-

grids in the Seoud & Vassilicos 2007 experiments requires a large number of grid points. Nagata *et al.*(2008) and Laizet *et al.*(2008) made preliminary attempts to reproduce the experiments, further studies are necessary, in particular because the reproduction of the grid by the Immersed Boundary Technique could affect the results. In the present study an idea of the effect of the inlet conditions has been obtained by assigning large scale velocity distributions and small random noise disturbances. The simulations, without the interaction between flow and grids are more efficient from the numerical side. A comparison with the realistic simulations allow to draw some conclusions on the effect of the inlet conditions.

Numerical method

Basic finite difference

The basic numerics consists on a second order finite difference scheme with staggered velocities, which in the inviscid limits and for three periodic directions conserves the total energy. The method is described in Orlandi (2000), where are also shown the global conservation properties, for the inviscid equations. In such conditions, a comparison with a scheme forth order accurate and with the pseudospectral method was performed by Duponcheel *et al.*(2008) showing that second order accuracy is rather good, even if not better than the other methods. Slight modifications are necessary to solve the Navier-Stokes equations with two periodic directions and inlet outlet boundary conditions. The inlet conditions are easily assigned by an analytical expression for the three velocity components. At the outlet radiative conditions allow to the flow to exit from the computational domain without producing any disturbance propagating upstream.

The numerics, shortly resumed, allow to solve the incompressible non-dimensional Navier-Stokes and continuity equations given by

$$\frac{\partial U_i}{\partial t} = -\frac{\partial U_i U_j}{\partial x_j} - \frac{\partial P}{\partial x_i} + \frac{1}{Re}\frac{\partial^2 U_i}{\partial x_j^2} = RHS_i\,; \qquad \frac{\partial U_i}{\partial x_i} = 0\,, \tag{1}$$

where the reference velocity is the uniform U_0 at the inlet and the reference length is such that the square computational section, orthogonal to x_1, has sides of length $L_2 = L_3 = 2\pi$.

Analytical inlet conditions

For the simulations without solid grids within the flow, the non-dimensional inlet velocity are

$$U_l = \delta_{1l} + A_l \sin(Nx_2)\sin(Nx_3) + A_R(x_2, x_3) \tag{2}$$

where A_l is the amplitude of the large scale disturbances set equal to 0.25 only for $l = 2$ and $l = 3$ and $A_R = 0.01$ is the amplitude of small random disturbances. To investigate the effects of the solidity of single scale grids three cases with N equal to $2, 4$ and 8 have been considered, and are indicated by I_N. To have an idea of the modification of the streamwise evolution by a multiscale grid N has been varied in different sectors of the inlet section. In these circumstances the flows are indicated by I_M at low and I_H at high Re numbers. For the U_1 component only a random disturbance is added to the uniform stream. An uniform mesh in the three directions has been used with resolution $2\pi/160$. To evaluate the decay rate correctly and to investigate whether the turbulence becomes isotropic the computational domain should be long enough. For $N = 8$ and $L_1 = 12\pi$, $L_1/M = 48$, a sufficiently long distance, comparable to that in laboratory experiments.

Real simulations

To reproduce numerically the effects of a grid it is necessary to add to the basic numerical method the Immersed Boundary Technique. The method here used was applied by Leonardi & Orlandi (2004) to rough channels flows, the difference is that here a mean pressure gradient is not necessary; the constant flow rate is obtained by adjusting the outlet conditions. Even if, in principle, grids with holes of any shape can be treated, here the study is restricted to rectangular holes. The size of the void is equal to w, that of the solid equal to b and the thickness of the grid is equal to k.

For these real simulations the inlet velocity U_1 must be assigned at a distance L_g ahead of the grid, therefore the outlet boundary has been imposed at $L_1 = 24\pi$. In these simulations 192 points in x_2 and x_3, have been used, accordingly the number of points in x_1 are 1536. The flow past the grid becomes turbulent or not depending on the solidity of the grid. It has been found that for a grid composed by by 8×8 elements; for small solidity ($b = 4\pi/192$) and $w = 44\pi/192$) the flow does not become turbulent, while for large solidity ($b = 16\pi/192$ and $w = 32\pi/192$) isotropic turbulence is obtained at distance $x_1/M > 10$. The shape of the grid dictates the velocity distribution at the exit of the grid. For the two grids here considered one with a single scale and the other with multiple scales the U_1 and the U_2 distributions are different from those assigned by Eq.(2).

From these considerations our opinion is that the simulations described in the next section allow to have informations on the effects of the initial conditions on the generation of isotropic turbulence by a solid grid.

Results

Analytical and realistic simulations

In this paper more emphasis is given to the simulations with analytical disturbances at the inlet, however it is worth presenting a comparison with the more realistic conditions to evaluate their differences. The inset of Fig.1 shows the profiles of q in the two different type of simulations, for the analytical disturbances small oscillations occur, whereas for the realistic conditions q is zero at the inlet. Ahead the grid,q for single and multiple scale disturbances sharply increases, with minor differences, which become large after the grid. In the two cases there are large differences with a higher growth for a longer distance for the multiple scale grid. To make a comparison among the results it is necessary a normalisation with the reference value $q_0 = q(x_{10})$. For the analytical disturbances the natural choice for q_0 is at $x_1 = 0$, for the realistic simulations the values of x_1 in correspondence to the maximum of q have been chosen. The obtained profiles in Fig.1

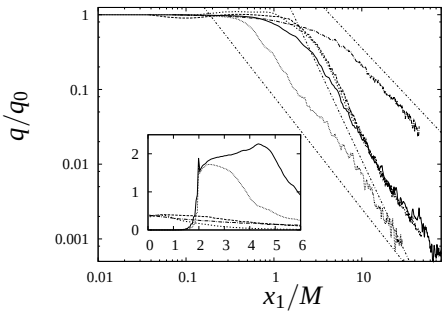

Figure 1. Profiles of q versus x_1/M scaled with $q_0 = q(x_{10})$ at different distances x_{10}, for analytical disturbances $x_{10} = 0$, for realistic grids: single scale $x_{10} = 2.33$ multiple scale $x_{10} = 4.34$: in the inset the profile of q in the initial region versus x_1,

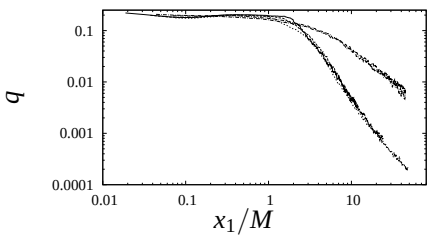

Figure 2. a) Profiles of q versus x_1/M: ——— I_2, – – – – I_4, ····· I_8, thick —·— I_M at different times, thin —·— I_H.

show different power laws in the isotropic region, in particular for the single scale disturbances at large distances from the grid, the slope is approximately $m = 2.5$. This slope was measured by Batchelor & Townsend (1948b) in the final period of decay when the R_λ is small. They defined different regimes accordingly to the parameter $22/R_\lambda$, that in the final period is greater than 1. On the other hand, Batchelor & Townsend (1948a), in a different paper, studied the initial period of decay with $22/R_\lambda < 1$ measuring a power law decay $m = 1$. In these circumstances R_λ is constant. Figure 1 shows that a power law $m = 1$ can always be found at a short distance, but to have a meaning the slope should last for a substantial distance. Even if $m = 1$ was not found for all the flows, $m = 1.25$ was achieved for the multiple scale disturbances, both by the real and by the analytical disturbances. In no one of the flows R_λ remains constant for a long distance even by increasing the Reynolds number. It can be then postulated that to get a constant R_λ an opportune shape of the grid should be designed. Perhaps the use of circular wires together with the large scale motions always present in closed circle wind-tunnels could be the reasons why Batchelor & Townsend (1948a) got $m = 1$. The present results with the multiple scale disturbances agree with those measured by Lavoie *et al.*(2007) . The profiles in Fig.1 suggest that the shape of the grid plays a fundamental role that requires more specific simulations.

Due to large dependence of the inlet disturbances on the statistics behaviour, in the next section, a more detailed analysis of different statistical quantities is presented for the flows with analytical disturbances.

Analytical inlet conditions

Velocity statistics The analytical distributions in Eq.(2) give $\langle u_l^2 \rangle = O(10^{-1})$ for $l = 2$ and $l = 3$ and $\langle u_1^2 \rangle = O(10^{-3})$ having also $\langle u_2 u_3 \rangle \neq 0$, a condition far from the isotropic one $\langle u_2 u_3 \rangle = 0$. The initial disturbance at $x_1 = 0$ is convected downstream and, at a certain time, reaches the outlet section. Only at that time the fields can be saved to have a greater number of samples, necessaries to get well converged statistics. To understand the streamwise approach to isotropy here some of the statistics are evaluated with one realisation.

From a qualitative point of view the increase of N in Eq.(2) is associated to disturbances at smaller scales which decay faster in x_1. The mean streamwise velocity U_1 is constant in x_1 then, one is expecting that the propagation velocity of the disturbances should not vary with N. On the other hand, it has been observed that, the disturbances with small N propagate faster, even without large differences on the time when the disturbances reach the end of the domain. A global picture of the streamwise decrease of the energy disturbance q with x_1, demonstrates that, for single scale disturbances, the location where the turbulent energy begins to decay moves upstream with the increase of N. For multiscale the decay rate is different from that for single scale disturbances. To have the idea of the q variations in x_1 during the statistical steady state stage, the profiles of q for multiscale disturbances, at different times ($t = 60, 100$ and $t = 140$) overlap one to the other, each one presenting streamwise oscillations typical of turbulent flows.

In laboratory experiments the variations of the turbulent quantities were given in function of a distance normalised with the mesh size M of the grid, here given by $M = 2\pi/N$. By plotting q versus x_1/M the profiles of the single scale disturbances, from a certain point, overlay each other (Fig.(2)). The case I_8 shows, better than the others, variations of m in x_1, emphasising the influence of the length of the computational box in the determination of m. This was also found in laboratory experiments, for instance Lavoie *et al.*(2007) measured in a range $30 < x_1/M < 100$ greater than here. Then the present values of m are higher than the m by Lavoie *et al.*(2007) varying between 1.06 and 1.24. The present DNS show that for $1 < x_1/M < 3$ the q decay varies with N, and that for $3 < x_1/M$ an equal value for m is obtained. The differences in the regions of large anisotropy depending on the vortical structures can be understood by DNS.

The value of M for the multiscale disturbances has been evaluated as $M = (2+4+8+16)/(8\pi)$. The decay in Fig.(2) differs from that for the single scale disturbances, and it is rather difficult to imagine the existence of a value of M leading to a superposition of the two set of curves in Fig.(2). The results in Fig.1 reinforce this point, in fact an universal decay rate for multiple scale disturbances doe not hold. Figure (2) shows an initial decrease of q, which is due to the influence of the sectors with $N = 16$. The weak decay, in the isotropic region ($x_1/M > 10$), is due to the existence of the vortical structures generated by the sectors with $N = 2$.

The achievement of isotropic turbulence can be establish by looking at the turbulent stresses $\langle u_i u_j \rangle$, which, with the present inlet conditions have a correlation coefficient $C_{32} = \langle u_3 u_2 \rangle / \sqrt{\langle u_3^2 \rangle \langle u_2^2 \rangle} = 1$. This high C_{32} can not be achieved in real numerical experiments, as those above presented. Then these simulations with $C_{32} = 1$ are very useful to understand the transition from anisotropic to isotropic turbulence. The turbulent stress $\langle u_3 u_2 \rangle$ can have positive or negative values, in particular when it is small, therefore to analyse the sharp de-

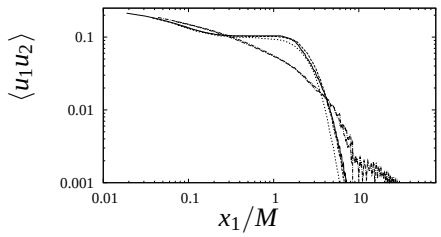

Figure 3. Profiles of $|\langle u_1 u_2 \rangle|$, versus x_1/M: ——— I_2, – – – – I_4, ····· I_8, —·— tick I_M, —·— thin I_H.

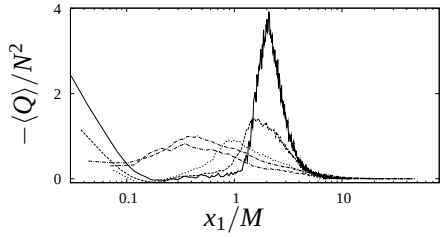

Figure 4. Profiles of $\langle Q \rangle$ scaled with respect to N^2 versus x_1/M , here $\langle Q \rangle$ at the high *Re* has been divided by 3 the ratio of the high and the low Reynolds numbers; ——— I_2, – – – – I_4, ····· I_8, —·— tick I_M, —·— thin I_H.

crease towards zero, it is preferable to plot the absolute value. The *Re* independence has been verified for single and multi-scale disturbances, but is shown, in Fig.(3), only for the multiscale disturbances. As for the normal stresses, the profiles of $|\langle u_3 u_2 \rangle|$ versus x_1/M indicate that isotropy is reached at a location x_1/M for the single scale disturbances (Fig.(3)). For the multiscale disturbances, even if the trend is different, it can be asserted that within a distance of five M isotropic turbulence is reached. Plots of the ratio $K = \langle u_1^2 \rangle / \langle u_2^2 \rangle$ demonstrate that a perfect isotropy is not achieved, and this can be related to the influence of the large scales on $\langle u_l^2 \rangle$.

Flow structures and streamwise stress

The streamwise momentum equation averaged in the two normal directions implies a balance between $\langle p \rangle$ and $\langle u_1^2 \rangle$. In addition, by averaging the Poisson equation for pressure - $\nabla^2 p = s_{ij} s_{ji} - \omega_i \omega_i / 2 = -Q$, we get

$$-\frac{\partial^2 \langle p \rangle}{\partial x_1^2} = -\langle Q \rangle = \langle s_{ij} s_{ji} \rangle - \langle \omega_i \omega_i / 2 \rangle = S - O = \frac{\partial^2 \langle u_1^2 \rangle}{\partial x_1^2} \tag{3}$$

From this equation it can be asserted that $\frac{\partial^2 \langle u_1^2 \rangle}{\partial x_1^2}$ controls the topology of the turbulent structures. To know which type of structures prevails we recall that points with $Q > 0$ are associated with tube-like, whereas points with $Q < 0$ are associated with sheet-like vortical structures (Tsinober 2009 Chapter 6). This statement has a physical meaning only when s_{ij} and ω_i are derived by velocity fields solution of the Navier-Stokes equations. It is important also to remind that s_{ij} and ω_i are the quantities entering in the vorticity transport equations. In isotropic turbulence $\langle Q \rangle = 0$ although the number of points with $s_{ij} s_{ji} > \omega_i \omega_i / 2$ is greater than those with $s_{ij} s_{ji} < \omega_i \omega_i / 2$. This occurrence produces a negative skewed probability density function of $\nabla^2 p$, implying that the most extreme events are associated to sheet-like structures (Ashurst et al. 1987). In the anisotropic part of the present flows $\frac{\partial^2 \langle u_1^2 \rangle}{\partial x_1^2}$ accounts for the disequilibrium between S and O; this term can, then, be regarded as a measure of the number of sheet-like structures, which being inherently unsteady, roll-up leading to the transition from anisotropic to isotropic turbulence. Figure (2) shows that, at $x_1/M \approx 3.5$, for all the N, $\langle u_1^2 \rangle \approx (x_1/M)^{-m}$, hence $\frac{\partial^2 \langle u_1^2 \rangle}{\partial x_1^2} \approx (x_1/M)^{-m-2}$ asserting that the tendency towards isotropic turbulence is rapid. For the flows at different N, the plots of $\langle Q \rangle$ versus x_1 show a prevalence of sheet-like structures. For the multiscale disturbances the disequilibrium increases with the Reynolds number, but by multiplying $\langle Q \rangle$ for the *Re* numbers ratio there is a better similarity. These plots indicate that, by increasing N, the sheet-like structures form closer to the inlet and that these prevail for a longer distance for multiple scale disturbances. The $\langle Q \rangle$, normalised with N^2 and plotted in Fig.(4) versus x_1/M, in agreement with the previous observations, shows that isotropic turbulence forms at the same x_1/M and that the structures disequilibrium increases by reducing N. This is reasonable because low N generate larger structures which are more unstable.

Lamb vector For a better understanding in the anisotropic and in the isotropic regions the streamwise mean momentum equation, where $\frac{d\langle u_1^2 \rangle}{dx_1}$ balances $\frac{d\langle p \rangle}{dx_1}$, has been considered. For the flows I_2 and I_8 the terms scaled with N, and plotted versus x_1/M, indicate a similar behaviour near the inlet and some difference in the anisotropic region. To have more informations is worth to write the momentum equation in rotational form, where q enters, and then it is possible to distinguish the different contributions to the q variations in the anisotropic and in the isotropic regions. The momentum equations in this formulation are

$$\frac{\partial U_i}{\partial t} - \varepsilon_{ijk} U_j \omega_k = -\frac{\partial \phi}{\partial x_i} + \frac{1}{Re} \frac{\partial^2 U_i}{\partial x_j^2} \tag{4}$$

with $\phi = p + U_i^2/2$. By averaging the equation in the x_2 and x_3 directions the equation for the streamwise component $\langle U_1 \rangle = 1$ is

$$\frac{\partial q}{\partial x_1} - \langle u_2 \omega_3 \rangle + \langle u_3 \omega_2 \rangle = -\frac{\partial \langle p \rangle}{\partial x_1} = \frac{\partial \langle u_1^2 \rangle}{\partial x_1} \tag{5}$$

It is, then, possible to distinguish the contribution of the different terms to the streamwise variations of q or $\langle u_1^2 \rangle$. The right hand side of this equation indicates that the pressure gradient drives the growth of $\langle u_1^2 \rangle$. This stress is absent at $x_1 = 0$, and had to grow to become comparable to the other stresses. The equal magnitude of the stresses is the first requirement to fulfil to have isotropic turbulence. The pressure gradient is given by the external force necessary to maintain a constant flow rate, and consequently a constant total energy. The

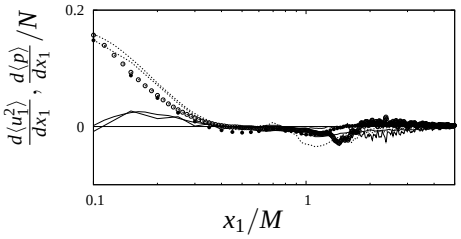

Figure 5. Profiles of the terms in the equation for the mean streamwise momentum equation $\frac{d\langle u_1^2\rangle}{dx_1}$ – – – – decomposed in $\frac{dq}{dx_1}$ ——— and the streamwise component of the Lamb vector λ for I_8 tick lines and solid circle, for I_2 thin lines and open circle

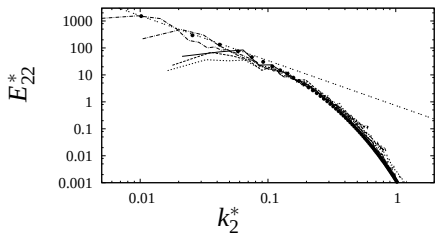

Figure 6. Profiles of dimensionless one-dimensional longitudinal spectra in Kolmogorov variables: at $x_1/M = 10$; ——— I_2, – – – – I_4, ····· I_8, —·— tick I_M, thin I_H, solid circle forced isotropic turbulence at $R_\lambda = 100$ Jimenez *et al.* (1993).

components of the Lamb vector $\lambda = \mathbf{v} \times \omega$ are related to the rate of energy transfer from large to small scales. Figure 5 shows a large increase of $\langle u_1^2 \rangle$ at the entrance which reduces becoming negligible at $x_1/M \approx 0.3$. Figure 5 shows that q does not largely vary in the first region, and from Eq.(5) it follows that the increase of $\langle u_1^2 \rangle$ is due to the contribution of the Lamb vector. From a control point of view this observation, suggests that a delay of the transition to isotropic turbulence can be achieved by applying an external force aligning the velocity and the vorticity vectors. This mechanism has been studied by Orlandi (1997) in rotating pipes where the rotation increases the helicity density $h = \mathbf{v} \cdot \omega$, which from the identity $|\mathbf{v} \times \omega|^2 + |\mathbf{v} \cdot \omega|^2 = |\mathbf{v}|^2 |\omega|^2$ reduces the transfer from large to small scales. Several studies have demonstrated that by adding solid body rotation to isotropic turbulence the decay rate decreases (Davidson 2010). The Eq.(4) helps to understand why the energy decay rate reduces by increasing the rotation rate. Numerical experiments on the effect of solid body rotation for the flow I_8 are currently performed and the results will be presented in a different paper.

The strong anisotropic region ends at $x_1/M \approx 0.3$, in the successive region the three normal stresses are constant, but $\langle u_1^2 \rangle$ is greater than the other two. To reach the isotropic state $\langle u_1^2 \rangle$ should decrease with a rate depending on N. Figure (5) shows that the decrease is equally due to $\frac{\partial q}{\partial x_1}$ and to $-\langle u_2 \omega_3 \rangle + \langle u_3 \omega_2 \rangle$.

Velocity spectra In laboratory experiments the velocity spectra are evaluated by a single wire probe and the time signal is processed by using the Taylor hypothesis. The same procedure is feasible in the numerical simulations at the expenses of a large CPU necessary to have a long time signal oscillating around the statistical steady state mean value. In the numerical simulations, the spectra can also be evaluated in the two homogeneous directions (x_2 and x_3). Having the true longitudinal and transverse spectra and those from the time signals it could be interesting to verify the validity of the Taylor hypothesis. This comparison is presented elsewhere; here the interest is to compare the longitudinal and the transverse one-dimensional spectra with those obtained in forced isotropic turbulence. The longitudinal and transverse spectra can be evaluated by using different velocity components which should produce the same results. To demonstrate that this is indeed verified has been considered the I_H flow, which produces wider spectra than I_M. It has been verified that the longitudinal spectra $E_{22}(k_2)$ and $E_{33}(k_3)$ are equal at a distance $x_1/M = 10$. Instead these plots, at a distance $x_1/M = 2$, show a small anisotropy persistence at large scales. As it should be expected, the isotropy is achieved, before at small and later on at large scales, this is demonstrated by the transverse spectra, where, at the large scales, some anisotropy is still present at $x_1/M = 10$.

The comparison with the spectra in forced isotropic turbulence necessitates the spectra in Kolmogorov variables. The rate of dissipation ε has been calculated by the one-dimensional spectra ($\varepsilon = 15\nu \int k_l^2 E_{ll} dk_l$), the Kolmogorov scale is $\eta = (\varepsilon/\nu^3)^{1/4}$, the non-dimensional wave number is $k_l^* = k\eta$, and the one-dimensional dimensionless spectra are $E_{ll}^* = E_{ll}(\varepsilon/\nu^5)^{-1/4}$. The sharp energy peaks in the spectra at $x_1/M = 2$ (not reported), separated by a wave number proportional to N, indicate the effect of the inlet disturbance. This implies that the energy inserted at the wave number of the disturbance has not been transferred into the whole range of wave numbers. Therefore the smallest dissipating Kolmogorov scales, are not formed, as emphasised by the deviations, from the correct exponential range. On the other hand, further downstream, at $x_1/M = 10$, Fig. (6) indicates a collapse of all the spectra in the exponential range with those obtained by the Jimenez *et al.*(1993) pseudospectral simulations. The outcome of this figure is that for the I_H flow isotropic turbulence at a reasonable high R_λ was generated. Instead, at the same Reynolds number, single scale disturbances were producing turbulent flows at low R_λ. From the numerical side the spectra confirm that the flow is well resolved and that these numerical experiments generate flows similar to those by grids in wind tunnels.

Conclusions

The simulations described in this paper were devoted to have a better understanding of the effects of the type of the grid on the flows paste grids. It has been demonstrated that grids with a single scale mesh generate flows having a turbulent energy decaying with a power law $m = 2.5$. This high value is typical of turbulence at small R_λ (Batchelor & Townsend (1948b), where the energy spectra are dominated by the exponential range. To have insights on the effect of the grid solidity, simulations with analytical inlet disturbances, having two large normal stresses and the third null, were per-

formed. These inlet conditions far from the isotropy, lead to a better understanding on the approach to isotropy. A good scaling of the normal stresses with the size of the disturbance was found, and it was, also, observed that this scaling does not old for the statistics of the vorticity in the whole downstream direction. The terms of the streamwise momentum equations indicate large scale effects close to the inlet, due to the pressure difference necessary to maintain a constant flow rate. Further downstream the effect of the energy transfer from the large to the small scales is predominant, which has been analysed by the momentum equation in rotational form. The appearance of the Lamb vector suggests an eventual control of the power law decay rate, through the alignment of the velocity and the vorticity vectors, which can be obtained by solid body rotation. The reduction of the decay rate has been observed in preliminary simulations, which were not discussed, and will be presented elsewhere.

The comparison between simulations with single and multiple scale disturbances demonstrated the possibility to reduce m, but a long region with $m = 1$ was not found. Batchelor & Townsend (1948a), in their early experiments, obtained $m = 1$, characterised by a constant R_λ, which is of interest in practical applications. The present simulations, indeed produced higher R_λ, corroborating the results in experiments with fractal grid (Seoud & Vassilicos 2007) and suggesting the necessity of more numerical simulations. The different behaviour of single and multiple scale disturbances, and, in particular, the difficulty to get $m = 1$ with single scale disturbances, suggests the presence of multiple scale disturbances in laboratory experiments with regular grids. These could be due to fabric imperfections on the grid, and to large scale flow disturbances in the wind tunnels.

In this study the multiple scale disturbances were also created by a real simulation and it was observed that the values of m differ from that obtained by analytical distributions, this is a further evidence that the shape of the grid plays an important role on the decay of isotropic turbulence.

The comparison of the spectra, in Kolmogorov units, with those obtained by pseudospectral simulations of forced turbulence shows that R_λ is comparable. The present flows are generated as in the experiments and by knowing not only the velocity but also the pressure and the vorticity fields can be of help to the experimentalists. For instance, at a desired location, the time variations of the variables can be stored, and by using the Taylor hypothesis the longitudinal and transverse spectra can be evaluated and compared with those in the homogeneous directions. The spectra evaluation by arrays of probes is expensive in laboratory experiments, then the present simulations can be of help to investigate the validity of the Taylor hypothesis. In the recent years vorticity probes have been used, (Wallace & Vukoslavcevic 2010) but rarely their configuration has been reproduced in numerical simulations to investigate the limitations of the probes. The flows here studied are candidate to this purpose.

Acknowledgments

The support of a MIUR 60 % grant is acknowledged; the computer time was given by CASPUR

REFERENCES

Ashurst, W.T. , Kerstein, A.R, Kerr, R.M. and Gibson, C.H., 1987, "Alignment of vorticity and scalar gradient with strain rate in simulated Navier–Stokes turbulence" Phys. Fluids Vol. 30, pp 2343–2353.

Batchelor G. K. and Townsend A.A., 1948 "Decay of Turbulence in the Final Period" Proc. R. Soc. Lond. A, Vol. **194**, pp. 527-543

Batchelor G. K. and Townsend A.A., 1948 "Decay of Isotropic Turbulence in the Initial Period" Proc. R. Soc. Lond. A, Vol. **193**, pp. 539-558

Davidson, P.A.,2010, "On the decay of Saffman turbulence subject to rotation, stratification or an imposed magnetic field" J. Fluid Mech, Vol. **663**, pp. 268 - 292.

Djenidi, L. 2006 "Lattice-Boltzmann simulation of a grid-generated turbulence" Journal of Fluid Mech, Vol. **552** , pp. 13 - 35

Duponcheel, M., Orlandi, P. & Winckelmans, G. 2008 "Time-Reversibility of the Euler Equations as a Benchmark for Energy Conserving Schemes" J. Comp. Physics, Vol. **227**, pp 8736-8752.

Ertunc, O., Ozyilmaz, N., Lienhart, H., Durst, F. & Beronov, K.,2010 "Homogeneity of turbulence generated by static-grid structures" Journal of Fluid Mech, Vol. **654** ,pp. 473 - 500 .

Jimenez, J., Wray, A. A., Saffman, P. G. & Rogallo, R. S. 1993 "The structure of intense vorticity in isotropic turbulence" J. Fluid Mech, Vol. **255**, pp 65-90, the data are available in AGARD AR-345 1998.

Hurst, D, and Vassilicos, J. C., 2007 "Scalings and decay of fractal-generated turbulence" Phys. Fluids, Vol. 19, pp. 035103

Laizet, S., Lamballais, E. and Vassilicos, J.C., 2008 "A numerical strategy to combine high-order schemes, complex geometry and parallel computing for high resolution DNS of fractal generated turbulence" Computer & Fluids, Vol.bf 39, pp.471-484.

Lavoie, P., Djenidi, L. and Antonia, R.A. 2007 "Effects of initial conditions in decaying turbulence generated by passive grids" Journal of Fluid Mech, Vol.**585** , pp. 395 - 420

Leonardi, S, and Orlandi, P., 2004 "DNS of turbulent channel flows with two- and three-dimensional roughness" Journal of Turbulence., Vol. **7**, No. 53

Nagata, K., Suzuki, H., Sakai Y., Hayase, T. and Kubo, T., 2008 "Direct numerical simulation of turbulent mixing in grid-generated turbulence" Phys. Scr. T132 014054

Orlandi, P. 1997. "Helicity fluctuations in rotating and non-rotating pipes" Phys. Fluids, Vol. **A 9**, 2045–2056.

Orlandi, P. 2000. *Fluid Flow Phenomena : A Numerical Toolkit*, Kluwer.

Seoud, R. E. & Vassilicos, J. C., 2007 "Dissipation and decay of fractal-generated turbulence" Phys. Fluids, Vol. 19, pp. 105108

Tsinober, A., 2009 *An Informal Conceptual Introduction to Turbulence* Second Edition, Springer

Wallace, J.M. and Vukoslavcevic, P.V., 2010 "Measurement of the Velocity Gradient Tensor in Turbulent Flows" Annual Review of Fluid Mechanics, Vol. 42 , pp 157–181